Biomaterials Science

ROYAL SOCIETY OF CHEMISTRY

PAPER

View Article Online
View Journal | View Issue

Cite this: *Biomater. Sci.*, 2025, **13**, 2673

Gradually-frozen aligned bacterial nanocellulose membranes loaded with gallic acid exhibit enhanced mechanical and dual antithrombotic-antimicrobial properties†

Emma D. Stephens,[a] Fereshteh Oustadi,[a] Hunter Marcelo,[a] Jaqueline L. Vierra,[a] Kartikeya Murari,[a,b] Philip Egberts[c] and Maryam Badv *[a,d]

Received 6th February 2025,
Accepted 26th March 2025

DOI: 10.1039/d5bm00176e

rsc.li/biomaterials-science

Bacterial nanocellulose (BNC) is a versatile natural polymer with unique morphological properties. However, its susceptibility to biofouling limits its utility in healthcare. To address this challenge, this study explores the incorporation of gallic acid, a phenolic acid with potent antimicrobial and antithrombotic properties, into BNC membranes. Additionally, a novel drying method termed gradual freezing is introduced, resulting in a directionally-aligned BNC membrane with enhanced mechanical integrity and high porosity. Using glycerol as a solvent and plasticizer, gallic acid was loaded into air-dried BNC (AD-BNC), freeze-dried BNC (FD-BNC), and gradually-frozen BNC (GF-BNC) membranes. Successful drug-loading into FD-BNC and GF-BNC significantly increased the elasticity of the films, however mechanical testing indicated that GF-BNC and its gallic acid/glycerol loaded counterpart (GF-GG-BNC) achieved overall optimal mechanical strength and elasticity. These samples were selected for further antifouling testing. Antibacterial assays demonstrated the practical efficacy of GF-GG-BNC in inhibiting the proliferation and biofilm formation of *E. coli* and *S. aureus*, while favorable antithrombotic behaviour prevented clot formation and red blood cell adhesion on the material's surface when compared to GF-BNC membranes. These findings highlight the potential of GF-GG-BNC as a multifunctional biomaterial for the prevention of biofouling in biomedical applications.

Introduction

Bacterial nanocellulose (BNC) is a versatile natural polymer synthesized by cellulose-producing bacteria such as *Komagataeibacter hansenii* from the *Komagataeibacter genus*.[1–3] BNC consists of micro and nanoscale cellulosic fibrils which create a three-dimensional matrix,[4] imparting unique morphological properties, making it of significant interest in biomedical research.[5–7] BNC is known to be naturally biocompatible with excellent water retention capacity, thermal stability, renewal potential, and shapability.[8] In addition, this natural hydrogel has been found to be non-cytotoxic and non-immunogenic.[9,10] BNC is a comparatively pure form of cellulose when contrasted with plant-based celluloses, which are known to contain impurities such as lignin, pectin, and hemicellulose.[11] This innate purity greatly reduces the requirement for costly and extensive purification procedures.[12] These unique properties have made BNC a material of interest for a variety of biomedical applications, including for wound dressings,[8,13,14] drug delivery,[15–18] and vascular graft applications.[19,20] With increasing interest in using BNC as a biomaterial, the industrial scale-up of BNC production and processing has also become a popular research topic,[21–23] increasing in-turn the relevance of BNC-based biomaterials. Despite the unique properties of BNC, the applications of pure BNC in biofluid-contacting biomedical applications are limited due to its susceptibility to biofouling.[14,24] BNC lacks intrinsic antimicrobial properties and the ability to prevent bacterial adhesion, proliferation, or biofilm formation, posing a risk of infection.[25] Furthermore, BNC has no innate anticoagulant properties, restricting its use in blood-contacting implants such as vascular grafts.[26] Current research is addres-

[a]*Department of Biomedical Engineering, Schulich School of Engineering, University of Calgary, Calgary, Alberta, T2N 1N4, Canada. E-mail: maryam.badv@ucalgary.ca*
[b]*Department of Electrical and Software Engineering, Schulich School of Engineering, University of Calgary, Calgary, Alberta, T2N 1N4, Canada*
[c]*Department of Mechanical Engineering, Schulich School of Engineering, University of Calgary, Calgary, Calgary, Alberta, T2N 1N4, Canada*
[d]*Libin Cardiovascular Institute, University of Calgary, Calgary, Alberta, T2N 4N1, Canada*

† Electronic supplementary information (ESI) available. See DOI: https://doi.org/10.1039/d5bm00176e

sing these limitations by introducing different surface engineering and bulk modification strategies, aiming to enhance the antifouling properties of BNC.

BNC is a porous material with abundant hydroxyl groups, allowing it to be post-modified for its target application.[20,27,28] Previous research has investigated both physical and chemical modification techniques for BNC, often focused on enhancing the material's antifouling or mechanical properties.[15,29–32] As a pure material with simple surface chemistry, a variety of chemical modifications have been applied to BNC to increase its applicability as an antifouling material. In our previous work, we presented the addition of a stable lubricant-infused layer on the surface of BNC membranes preventing the adhesion of bacteria, blood proteins and cells, water, and oils.[26] The lubricant-infused layer is immobilized on the surface of the BNC through a high chemical affinity between silane groups. In addition to chemical modifications, physical surface modifications have also been extensively studied to enhance the functionality of BNC.[33,34] One approach involves altering the surface morphology of the material, such as creating a wrinkled or textured surface. Surface wrinkling has shown to improve the mechanical properties, thermal stability, and crystallinity of BNC,[35] making the membranes more suitable for applications where strength and stability are of concern. Drug-loading techniques have been explored as a non-chemical modification method of endowing BNC with antifouling properties.[16,17,27] By incorporating drugs directly into the hydrogel matrix, BNC can serve as a drug-release platform for therapeutic agents.[36] One such study explored BNC as a potential shelf-stable material for delivering four different active pharmaceutical ingredients, demonstrating a three-month stability when loaded with caffeine, ibuprofen, diclofenac, and lidocaine.[17] This physical approach allows for the localized delivery of active drugs to targeted areas without the need for chemical bonding, offering advantages in applications such as wound healing, targeted pain relief, or hemostasis.[37–39] Recent research into BNC modifications has been of interest in the field of biomaterials, though the development of multi-functional BNC-based biomaterials with both antibacterial and antithrombotic properties remains critically underreported.

To increase the efficiency of modification techniques, BNC hydrogels are commonly dried prior to their application.[18,40] Typically employed drying methods include air-drying, oven-drying, or freeze-drying.[41] Both air-drying and oven-drying BNC pellicles rely on slow/semi-slow evaporation to remove water from the cellulose matrix, resulting in membranes with similar morphological properties.[41] As water slowly evaporates, the pores collapse and hydrogen bonding occurs between the hydroxyl groups within the fibers.[41] This results in a thin and brittle, yet mechanically strong membrane with significantly reduced porosity compared to non-dried BNC.[42] In applications such as tissue engineering or drug-loading where retaining the porous microstructure of BNC is required, freeze-drying BNC may be employed. To freeze-dry BNC, the material is rapidly frozen in a bath of liquid nitrogen or dry ice and ethanol, then lyophilized to sublimate ice from the pores of the material. The resulting membrane is porous and spongy, however there is evidence that rapidly freezing the BNC membranes may result in decreased mechanical integrity (ESI Fig. 1†).[43] An optimized material for drug loading applications should have a combination of the properties seen in freeze-dried and air-dried BNC; a material that is able to withstand mechanical stresses, with a porous microstructure capable of significant fluid retention.[44,45] To address the shortcomings of these materials, novel drying methods may be explored.

Another significant shortcoming of BNC is its lack of natural antifouling characteristics,[19,46,47] meaning that biointeractions (*e.g.*, with blood or bacteria) could potentially lead to biofouling complications, such as clot formation or biofilm development, thereby decreasing its utility in biofluid-contacting biomedical applications. To decrease risk of infection, patients receiving biomaterial implants are routinely placed on broad-spectrum antibiotics.[48] However, antibiotic-resistant bacteria are creating cause for concern in healthcare, leading to a significant rise in healthcare-associated infections.[49,50] To address the rise in antibiotic resistance, the use of bacteriophages,[51,52] new antibiotics,[53,54] and localized treatments[55,56] are currently on the leading edge of biomedical research. Drug-loaded materials can decrease or eliminate the need for systemic treatments to prevent biofouling while providing an increased localized drug dosage.

Gallic acid is a naturally occurring phenolic acid found in a variety of plant components, including bark, leaves, berries and herbs.[57,58] It is known to be a powerful antioxidant and active antimicrobial agent and has demonstrated potential in anti-cancer and anti-thrombotic applications.[59–63] Recent studies have investigated the potential for gallic acid to be integrated into a variety of materials, especially hydrogels, for uses in food packaging and biomedical applications.[64–68] These studies have highlighted the promising attributes of gallic acid in hydrogels, including antioxidant and antifouling activity. Gallic acid has been successfully incorporated into several hydrogels during synthesis, however, *in situ* drug loading with BNC is not feasible as the antibacterial nature of gallic acid could inhibit the formation of BNC membranes by disrupting the cell membrane of cellulose-producing bacteria.[69] For applications where drug-loading occurs post-synthesis, a solvent may be used. Though gallic acid has limited solubility of 11.5 g L^{-1} in water, it demonstrates increased solubility of 100 g L^{-1} in glycerol.[70] In this instance, glycerol not only increases the dose of gallic acid that can be loaded into the BNC membranes, but could act as a plasticizer, increasing the elasticity of the material.[71,72]

In this research, we present a multifunctional BNC membrane with strong mechanical properties and dual antifouling capabilities, effectively preventing bacterial adhesion and attenuating plasma clotting. A novel BNC drying method, termed gradually-frozen BNC (GF-BNC), is designed to retain the porous microstructure of BNC hydrogels without significant mechanical compromise. Wet BNC membranes are subjected to a controlled cooling rate of −1.5 °C min^{-1} until

frozen and were left in a −80 °C freezer overnight. Subsequently the samples were lyophilized to remove ice from the pores of the material. As a result of the gradual freezing process, the internal cellulosic structures within GF-BNC become directionally aligned. This alignment, along with the ability of gradual freezing to preserve the mechanical integrity of BNC by preventing micro/macro fractures during the freezing process significantly improved the mechanical strength of GF-BNC membranes when compared to freeze-dried BNC (FD-BNC) without collapsing the porous ultrastructure, as seen in air-dried BNC (AD-BNC). Furthermore, AD-BNC, FD-BNC, and GF-BNC membranes were loaded with gallic acid using glycerol as a solvent (GG) to create AD-GG-BNC, FD-GG-BNC, and GF-GG-BNC, respectively. The GG-loaded materials were characterized and mechanically tested along with the AD-BNC, FD-BNC, and GF-BNC membranes, providing clarity on the efficacy of GG loading for each drying method. Based on the results, the most promising GG-loaded material, GF-GG-BNC, was subjected to a series of antifouling experiments. The careful selection of drying method and subsequent loading with GG, resulting in GF-GG-BNC, yielded a highly elastic, anti-fouling material appropriate for biomedical applications.

Materials and methods

Materials

Gallic acid (97.5–102.5%, titration), calcium chloride, sodium chloride, 4-(2-hydroxyethyl)-1-piperazineethanesulfonic acid (HEPES), phosphate buffered saline (PBS) tablets, and glycerol (≥99.0%) were all purchased from Sigma-Aldrich. Gibco™ Bacto™ yeast extract, Gibco™ Bacto™ tryptone, Gibco™ Bacto™ peptone, agar powder, glucose, citric acid (>99%) were purchased from ThermoFisher Scientific Inc. Sodium hydroxide (NaOH) was purchased from Fisher Bioreagents, and sodium phosphate dibasic was purchased from ChemCruz™ ICN Biomedicals Inc. *Escherichia coli* (*E. coli*; ATCC 25922) and *Staphylococcus aureus* (*S. aureus*; ATCC BAA-41) strains were obtained from Cedarlane Laboratories. *Komagataeibacter hansenii* (*K. hansenii*; ATCC 53582) and GFP-tagged *E. coli* (25922GFP) were purchased from ATCC Co. Human whole blood was collected from healthy human donors. A citrated plasma pool was made using donations from at least five participants according to a protocol established previously.[73] All experiments were performed in accordance with the Guidelines of the Center for Phlebotomy Education, and experiments were approved by the Research Ethics Board committee at the University of Calgary (REB22-1151). Informed consents were obtained from human participants of this study.

BNC production, purification, and drying. To produce BNC, *K. hansenii* bacteria were inoculated into Hestrin–Schramm media in a large Petri dish. The dish was incubated at 30 °C for 5 days. After a thick pellicle was formed, the BNC was removed and purified in a bottle of 4 wt% NaOH at 80 °C with stirring. After purification, the BNC pellicles were subjected to a series of water rinses to remove all NaOH residue from the cellulose matrix. Water rinses were conducted at 4–8 hours intervals until the pH of the media was approximately 7. The purified BNC membranes were kept in distilled water at 4 °C until drying.

BNC membranes were dried in one of three ways. To freeze-dry the BNC pellicles, membranes were submerged into liquid nitrogen for 20–30 seconds, or until the pellicles were completely frozen. The frozen membranes were then lyophilized for 24 hours allowing for all ice within the matrix to sublimate, resulting in FD-BNC. AD-BNC was produced by allowing the membranes to dry at room temperature for 24–48 hours, resulting in a thin membrane. GF-BNC was produced by placing the BNC membranes into a chamber surrounded by isopropanol, which controlled the cooling rate to −1.5 °C min^{-1}. The chamber was placed in the freezer and cooled to −80 °C prior to lyophilization. Similar to FD-BNC, the samples were then lyophilized for 24 hours to remove all ice from the material.

Gradual freezing rate validation. To determine the cooling rate of BNC in the isopropanol chamber, temperature readings over time were taken with a thermistor at about a 1 Hz sampling rate. Data were received through MATLAB R2022 until the temperature plateaued (ESI Fig. 2a†). The decrease in temperature over time prior to membrane freezing was found to be −1.5 °C min^{-1}.

Gallic acid loading. To create the gallic acid solution, gallic acid powder was dissolved in pure glycerol at 10% (w/v). The BNC samples dried with different drying methods were stirred in the solution on a plate shaker at 160 rpm and 40 °C for 48 hours. To remove the excess non-loaded drug, the samples were agitated in water for ten seconds six times. The samples were then allowed to dry for 24 hours at room temperature prior to experimentation.

Atomic force microscopy (AFM). A Keysight Technologies Agilent 5500 AFM was operated in contact mode for all AFM images acquired using uncoated silicon probes (PPP-CONT, Nanosensors). Samples of each material were imaged in air at room temperature, with a scan area of 10 μm^2 and a tip scan speed of 1 $\mu m\ s^{-1}$. Picoview 2.0 and Gwyddion GPL software were used for data analysis,[74,75] in particular for the determination of Root Mean Square (RMS) roughness (R_q) from topographic images. The error has been presented as the standard deviation for each material.

Scanning electron microscopy (SEM). To prepare the samples for SEM, all samples were mounted on stubs using carbon tape and coated with 15 nm of gold using the Angstrom NexDep physical vapor deposition platform (Angstrom Engineering). SEM images were taken at multiple magnifications using a mixed scattered electron detector (60%) and background electron detector (40%) imaging modality using the Phenom XL G2 desktop SEM (Thermo Fisher Scientific). The porosity of FD-BNC and GF-BNC were determined from SEM images using ImageJ. Prior to sputter coating, biological samples were preserved in 4% formaldehyde for 24 hours and subsequently dehydrated with a

graded ethanol series of 50%, 70%, 80%, 90%, 95%, then two cycles of 100% ethanol. The samples were allowed to air-dry prior to sputter coating.

Attenuated total reflectance fourier transform infrared spectroscopy (ATR-FTIR). To assess the chemical bonds within the materials before and after the modification steps, ATR-FTIR analysis was performed using a Nicolet iS50 Spectrometer. Spectra were analyzed and compared using GraphPad Prism.

Tensile tests. Material behavior under tension was assessed using a UniVert uniaxial testing apparatus and data was collected using the UniVert software. The samples were cut into 1 cm × 3 cm pieces, and the ends of the samples were secured in the testing clamps. Prior to testing, the samples were subject to 0.1 N of pre-tension, and the width, thickness, and length of each sample were measured. The samples were stretched at a rate of 3 mm per minute until failure. The tests were imaged using a USB 2.0 monochrome scientific imaging camera (DMK 41AU02) at a rate of 10 Hz. An image-based principal strain analysis was conducted in the UniVert software, and the principal strain values were exported to a Microsoft Excel spreadsheet. A custom program written in MATLAB R2022 was used to map the principal strain on the surface of each sample type.

Twist tests. To assess the membranes' resistance to torsional stress, a twist test was conducted. Samples were cut into 1 cm × 3 cm pieces and clamped into the UniVert uniaxial testing apparatus. Samples were then subject to 1 N of pretension, and slowly twisted to failure, at which the total rotation was recorded in degrees. Due to machine limitations, any samples that exceeded the maximum rotation of 3600° were assigned such rotational value for analysis.

Gallic acid and glycerol loading in GF-BNC. GG loading in GF-BNC was assessed by monitoring the change in weight of GF-BNC membranes submerged in GG over time (ESI Fig. 2c†). GF-BNC samples were cut into 1 cm × 1 cm samples and their dry weight was recorded. While agitating the samples in 10% (w/v) GG at 40 °C, the change in weight of each sample was monitored periodically for 48 hours. To ensure that the weight of only absorbed GG was being measured, excess GG was removed from the surface of the samples by tapping them gently on a paper towel before recording their weight.

Gallic acid release from GF-GG-BNC. The release profile of GF-GG-BNC materials was characterized using UV-vis spectroscopy (ESI Fig. 2d†). In a 48-well plate, 1 cm × 1 cm samples of GF-GG-BNC were submerged in 800 μL of PBS at 37 °C. At each time point, the GF-GG-BNC samples were transferred to fresh PBS, and 200 μL samples from the previous wells were used to quantify gallic acid release using absorbance measurements from a plate reader (SpectraMax M2, Molecular Devices) from 200 nm–400 nm. A calibration curve was prepared to relate the concentration of the released gallic acid in PBS to the absorbance measurements, with a linear relation (R^2 > 0.97) observed in the concentration ranges of 5 mg mL^{-1} to 100 mg mL^{-1} for gallic acid. Cumulative gallic acid release of all repetitions was calculated and compared as a percentage of the release after 48 hours.

Disc diffusion test. To assess the antibacterial properties of the samples, disc diffusion tests were performed using both Gram-negative *E. coli* and Gram-positive *S. aureus*. Samples were cut into 8 mm circles using a biopsy punch. Colonies from each bacterial strain were previously isolated on a lysogeny broth (LB) agar plate, and one colony from each plate was separately suspended in 1 mL of LB broth. Using a sterile cotton swab, new LB agar plates were covered completely with the inoculated media. Samples were then placed on the bacterially inoculated agar plates and placed in an incubator at 37 °C for 30 hours. After the growth period, the plates were photographed and the zone of inhibition was measured using ImageJ. Samples from each plate were then preserved for SEM imaging.

Bacterial growth tests. The bactericidal properties of the membranes were further assessed using a bacterial growth test with both *S. aureus* and GFP-tagged *E. coli*. Samples were cut into 5 mm × 5 mm squares and suspended in 500 μL of bacterially inoculated LB media in a 48 well plate. An equal number of wells without samples were inoculated at the same time to act as a negative control. The light absorbance of the samples at 600 nm was used to indicate bacterial growth in a plate reader (SpectraMax M2, Molecular Devices), and fluorescent imaging was additionally used to visualize the quantity of GFP-tagged *E. coli* in the media surrounding the samples. Absorbance measurements were taken at inoculation, 4 hours, 12 hours, and 24 hours to assess bacterial growth over time. The absorbance of sterile LB media was recorded as a baseline and subtracted from all subsequent readings. The samples were kept in the incubator at 37 °C between readings. After 24 hours, samples from both groups were preserved for SEM imaging.

Plasma clotting assay. To assess the anti-clotting properties of the membranes, a plasma clotting assay was conducted. In addition to GF-BNC and GF-GG-BNC samples, GF-BNC treated with pure glycerol (GF-G-BNC) was tested to understand the contribution of glycerol to the anti-clotting nature of GF-GG-BNC. Samples were cut into 36 mm × 3 mm strips and placed around the circumference of the wells in a 48 well plate. To each well, 250 μL of citrated plasma was added, and the plate was then incubated at 37 °C for 10 minutes. To initiate clotting, 250 μL of 40 mM calcium chloride ($CaCl_2$) was added to each well, resulting in a final $CaCl_2$ concentration of 20 mM. Clotting was monitored manually for 4 hours, with samples removed from the wells in 2-minute intervals to detect clot formation. Time to clot was recorded when a cohesive clot could be seen in the well or attached to the sample. If no clotting occurred, clotting time was taken to be 4 hours. Samples were preserved for SEM imaging from each group after 4 hours.

Blood staining assay. Blood interactions with the materials were assessed using a blood staining assay. GF-BNC, GF-G-BNC, and GF-GG-BNC samples were cut into circles using an 8 mm biopsy punch and placed in a 48 well plate. The samples were then submerged in 500 μL of citrated whole blood for 45 seconds. After staining was complete, the samples were removed from the wells and tapped gently on a paper towel to

remove any blood that was not absorbed. The samples were then re-suspended in 700 μL of deionized water and agitated on the plate shaker at 240 rpm for 45 minutes to release any blood cells adhered to the surface. From each well, 200 μL of the solution was taken and added into a 96 well plate, and the absorbance was measured at 450 nm using a plate reader.

Statistical analysis. All data analysis was performed using GraphPad Prism. Graphical results are presented as mean ± standard deviation. All data presented is a cumulation of at least four repeats. To detect statistically significant results between two groups, a t-test was employed. One-way ANOVA was used to detect statistical significance between three or more groups.

Results and discussion

Microstructural and chemical characterization

BNC pellicles were grown using *K. hansenii* bacteria for 3–5 days and purified by soaking in 4 wt% NaOH at 80 °C while being stirred (Fig. 1a). After the pellicles were purified, the membranes were either air-dried, freeze-dried, or gradually-frozen (Fig. 1b and c). Each of these methods are explored in detail in the materials and methods section. To prepare AD-BNC, FD-BNC, and GF-BNC loaded with gallic acid (AD-GG-BNC, FD-GG-BNC, and GF-GG-BNC, respectively), each of the dried BNC membranes were submerged in a 10% (w/v) solution of gallic acid in glycerol for 48 hours. The samples were agitated on a plate shaker to promote the infusion of the drug throughout the material. To remove any excess drug from the surface of the membranes, they were shaken in distilled water for ten seconds for six cycles. The resulting AD-GG-BNC, FD-GG-BNC, and GF-GG-BNC samples were allowed to air-dry for 24 hours prior to experimentation, allowing for any residual water from the rinsing process to evaporate from the surface of the material (Fig. 1d).

Cross-sectional images of the samples were taken to provide understanding of how drying and GG loading affects the internal structures of AD-BNC, FD-BNC, and GF-BNC (Fig. 1c and d). The compact non-porous structure of AD-BNC

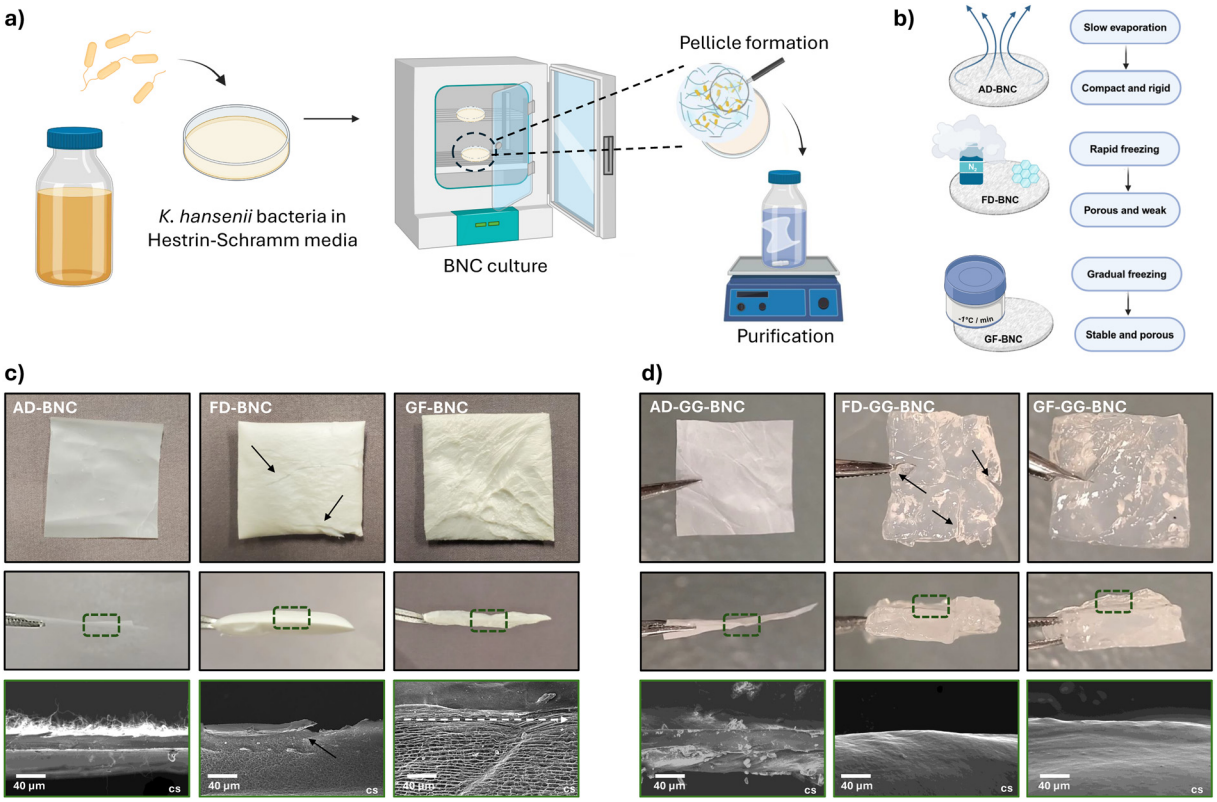

Fig. 1 (a) Schematic representation of BNC culture procedures, beginning with the inoculation of *K. hansenii* in Hestrin–Schramm media, followed by incubation for 3–5 days and subsequent purification. Created in BioRender. E. Stephens (2025). https://BioRender.com/4mcep01. (b) Different drying methods used to post-process the BNC membranes. Air-dried BNC (AD-BNC), freeze-dried BNC (FD-BNC) and gradually-frozen BNC (GF-BNC) membranes. Created in Biorender. E. Stephens (2025). https://BioRender.com/biwqiik. (c) Photographs and SEM images of samples after each drying method. Thermal fractures can be seen on the surface of the FD-BNC membrane. Cross-sectional SEM images of GF-BNC show an aligned microstructure, in contrast to FD-BNC, which exhibited a randomly aligned structure, and AD-BNC, where no pores were evident. (d) After drying, samples from each drying method were loaded with 10% (w/v) gallic acid using glycerol as a solvent. Similar to FD-BNC, FD-GG-BNC presents with fractures that can be seen on the surface. Cross-sectional SEM images confirm the incorporation of the GG layer in FD-GG-BNC and GF-GG-BNC samples.

is highlighted in Fig. 1c, where the entire cross-section of the material can be visualized. FD-BNC cross-section revealed a porous ultrastructure. This is expected as the rapid freezing and subsequent sublimation captures the native cellulose structure and prevents collapse of the material's pores. GF-BNC, however, reveals a different microstructure in its cross-section; as a result of the gradual freezing process, the internal fibres are directionally aligned. Directionally aligned polymers are coveted for their mass transfer capabilities and notable mechanical strength.[76,77] Both GF-GG-BNC and FD-GG-BNC show strong evidence of GG loading, with the pores of each material appearing confluent with GG loading (Fig. 1d). AD-GG-BNC, however, shows no visible sign of GG incorporation, with the cross-section appearing similar to that of AD-BNC.

To investigate the morphology, network structure, and surface roughness of BNC membranes after each drying method, AFM was performed. Contact-mode AFM was used to evaluate the surface topography and nanoscale roughness of AD-BNC, FD-BNC, and GF-BNC membranes (Fig. 2a and b). Each BNC sample displayed distinct topographical features that varied depending on the drying conditions. As shown in Fig. 2a, FD-BNC and GF-BNC presented similar fibre thickness and distribution, with GF-BNC fibres having marginally lower fibre thickness and more organization. These similarities were also evident in the measured R_q values of 37.34 ± 4.45 nm and 36.74 ± 2.39 nm for FD-BNC and GF-BNC, respectively. Consistent with other studies, AD-BNC exhibited a network of thinner, more densely packed fibres and yielded a significantly higher R_q of 46.47 ± 2.75 nm (Fig. 2b).[78,79] These surface measurements reflect the impact of water entrapment and water evaporation rate during drying on the resulting cellulose structure. In GF-BNC and FD-BNC, the formation and sublimation of ice displaces and enlarges cellulose fibres, causing higher porosity and looser fibrous strands. In contrast, the drying method for AD-BNC uses warmer temperatures and allows for slower water evaporation, which collapses the cellulose fibres into a compact network. These results demonstrate how different drying conditions directly influence the nanoscale surface properties and architecture of BNC membranes.

Further analysis of the surface topography and pore morphology of each of the dried BNC membranes as well as the GG loaded samples was conducted through SEM imaging (Fig. 2c). On the surface of AD-BNC, the cellulose fibers appear compact and undifferentiated from one another. This could be a direct result of how evaporation during air-drying affects the microstructure of BNC; during the slow evaporation, hydrogen

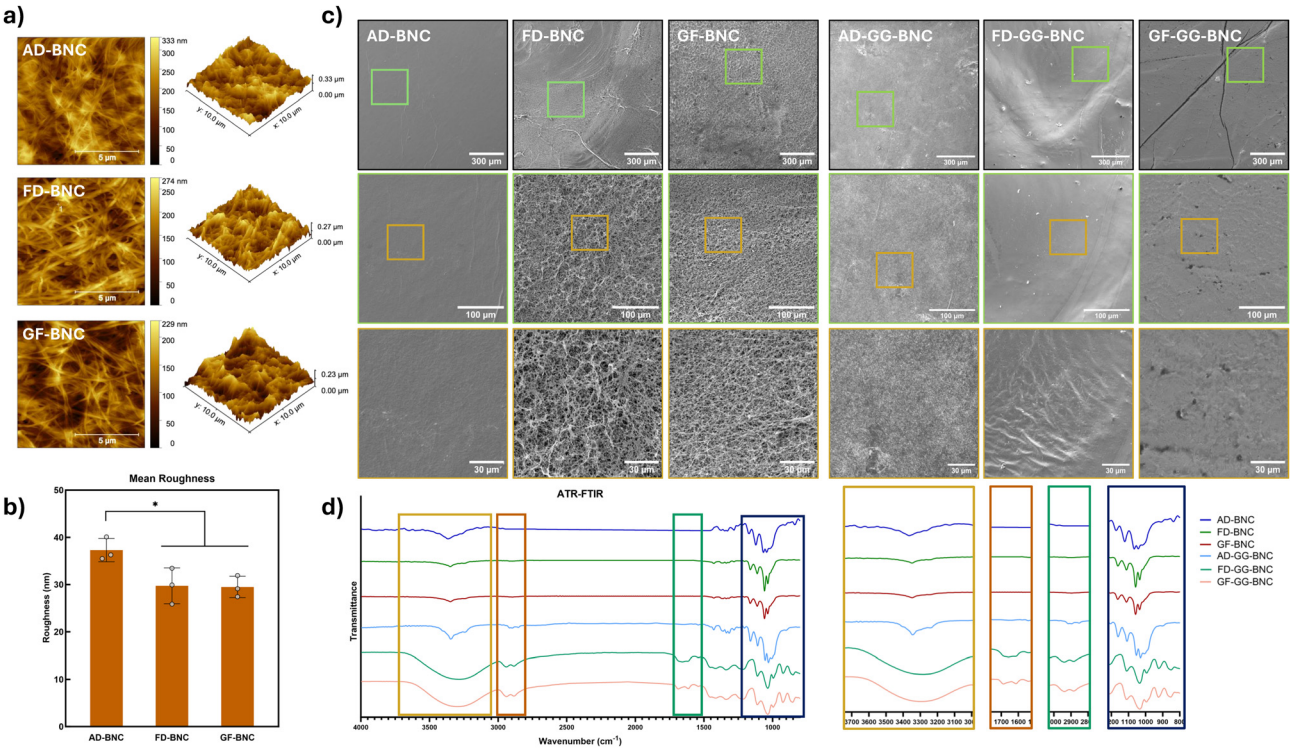

Fig. 2 (a and b) AFM topographical images were captured to determine 3D topography and RMS roughness for air-dried BNC (AD-BNC), freeze-dried BNC (FD-BNC) and gradually-frozen BNC (GF-BNC) membranes. (c) SEM images of each sample depict the microstructural differences seen between AD-BNC, FD-BNC, GF-BNC, and how being submerged in GG affects their surfaces. FD-GG-BNC and GF-GG-BNC membranes exhibit a confluent GG layer covering the porous structure of their dried counterparts. (d) ATR-FTIR spectroscopy analysis of AD-BNC, FD-BNC, GF-BNC, AD-GG-BNC, FD-GG-BNC, and GF-GG-BNC. AD-GG-BNC demonstrates –OH bending peaks similar to those of native BNC, not glycerol or gallic acid, indicating insufficient incorporation of GG. Data is represented as mean ± standard deviation. *$P \leq 0.05$.

bonding occurs within the material, promoting the compaction of cellulose fibers in AD-BNC.[80,81] This is in contrast with the surface appearance seen in both FD-BNC and GF-BNC samples, where the cellulose fibers are clearly differentiated from one another and the porous nature of the hydrogel is preserved. The pores on the surface of both FD-BNC and GF-BNC samples were of similar size, with most of the pores being less than 1 μm^2 (ESI Fig. 3a and b†).

The SEM images of the surfaces of the GG-loaded BNC membranes provide an indication of GG-loading efficiency. The surface appearance of FD-GG-BNC and GF-GG-BNC differ significantly from FD-BNC and GF-BNC, with the previously evident nanocellulosic structures being occluded with GG. The GG layer appears confluent on both surfaces, with small inhomogeneities existing where the pores of the material have absorbed GG into its inner matrix. Compared to AD-BNC, AD-GG-BNC does not present with significant microstructural changes. AD-GG-BNC strongly resembles AD-BNC as a compact surface with small amounts of fiber differentiation. This visual analysis provides a preliminary indication that GG incorporation in AD-GG-BNC may not be occurring to the same degree as seen in FD-GG-BNC and GF-GG-BNC.

The porosity of BNC directly correlates to several material properties. Prior to any drying procedure, cellulosic fibers in the BNC matrix are randomly distributed through space with water filling the pores of the material. Regardless of the drying procedure, the number of cellulose fibers in any cross-sectional point of the material will not change. However, upon drying, the volume that these fibers occupy may change drastically based on drying method (Fig. 1c). Mechanically, a more compact microstructure with dense cellulose fibers as seen in AD-BNC is expected to yield greater mechanical strength due to the increased hydrogen bonding between cellulose fibers and a decrease in empty space within the material.[82] These same hydrogen bonds will also increase the rigidity and brittleness of the material, decreasing its ability to deform elastically.[83] This compact microstructure is also hypothesized to decrease the GG loading capacity of AD-GG-BNC, as a lower porosity decreases the surface area in which the drug may stabilize, if it infiltrates the material at all.

To confirm successful incorporation of GG into each of the BNC membranes, all samples were examined using ATR-FTIR (Fig. 2d). Characteristic peaks seen in cellulose were visualized in AD-BNC, FD-BNC, and GF-BNC samples; bands at 665 cm^{-1}, 1015 cm^{-1}, and 1115 cm^{-1} are indicative of C-OH out-of-plane bending, C–C stretching, and C–O stretching, respectively.[26,84] Further, sharp peaks seen at 1420 cm^{-1} and 3350 cm^{-1} indicate C-H_2 bending and a characteristic absorption peak for cellulose.[3] While the ATR-FTIR spectra between the unmodified BNC samples were consistent with one another, cellulose-indicating peaks were mostly hidden by the presence of the GG components in FD-GG-BNC and GF-GG-BNC samples. Broad bands indicative of –OH stretching are typically seen around 3500 cm^{-1} for pure gallic acid[85] and 3320 cm^{-1} for glycerol.[86] The band seen in both FD-GG-BNC and GF-GG-BNC with a peak at 3300 cm^{-1} and a width spanning from 3650 cm^{-1} to 3000 cm^{-1} indicates the –OH stretching of both gallic acid and glycerol components while also hiding the typical cellulose characteristic peak at 3350 cm^{-1}. A pair of peaks at 2930 cm^{-1} and 2880 cm^{-1} demonstrating C–H stretching further indicate the presence of glycerol in the material. Gallic acid is further indicated in the ATR-FTIR spectra of FD-GG-BNC and GF-GG-BNC with the peak seen around 1670 cm^{-1}, demonstrating C=O stretching typically seen in phenolic acids.[87] The lack of characteristic peaks seen in cellulose with FD-GG-BNC and GF-GG-BNC are indicative of the abundance of both glycerol and gallic acid within the cellulose structures.

While the spectra of FD-GG-BNC and GF-GG-BNC clearly demonstrate a strong presence of gallic acid and glycerol components, there is significantly less evidence of them within the spectra of AD-GG-BNC. In the region around 3300 cm^{-1} where the broad characteristic peaks of –OH bending are seen for gallic acid and glycerol within FD-GG-BNC and GF-GG-BNC, a sharp peak that more closely resembles that of BNC can be seen in the AD-GG-BNC spectra. In addition to this, AD-GG-BNC also does not strongly present with a C=O peak around 1670 cm^{-1}, which indicates that there is not a significant presence of gallic acid within the sample. As mentioned previously, the successful GG-loading in FD-GG-BNC and GF-GG-BNC resulted in the lack of characteristic cellulosic peaks. The AD-GG-BNC spectra more closely resembles that of BNC than its GG-modified counterparts, with a sharp -OH bending peak at 3350 cm^{-1} and a C–H_2 bending peak at 1420 cm^{-1}.

Mechanical properties

To determine the mechanical characteristics of the BNC membranes dried with different techniques, a uniaxial tensile test was conducted. Samples were prepared in 1 cm × 3 cm pieces and loaded into a CellScale Univert uniaxial testing apparatus (ESI videos 1–6†). Once loaded, the samples were subjected to 0.1 N of pre-tension, and measurements were taken. Test data were used to develop stress–strain curves and principal strain maps for all samples (Fig. 3a and ESI Fig. 4†). The ultimate tensile strength (UTS), strain at rupture, and Young's modulus presented in Table 1 provide key insights into both the differences between drying methods and the efficacy of GG-loading between different sample groups (ESI Fig. 5†). As previously reported, AD-BNC demonstrates a mechanical advantage when compared to other drying methods.[22] The compact microstructure, as seen through both SEM and AFM visualization, directly contributes to an increase in mechanical strength and rigidity of the material, which is directly reflected with high UTS and Young's modulus values.[80] This is seen in direct contrast to FD-BNC, which has demonstrated limited mechanical integrity within this study. The mechanical integrity of GF-BNC is significantly improved compared to that of FD-BNC. While the UTS of the material is significantly lower compared to that of AD-BNC, GF-BNC demonstrates stable mechanical properties without compromising on its porous ultrastructure, which is key for drug-loading applications.

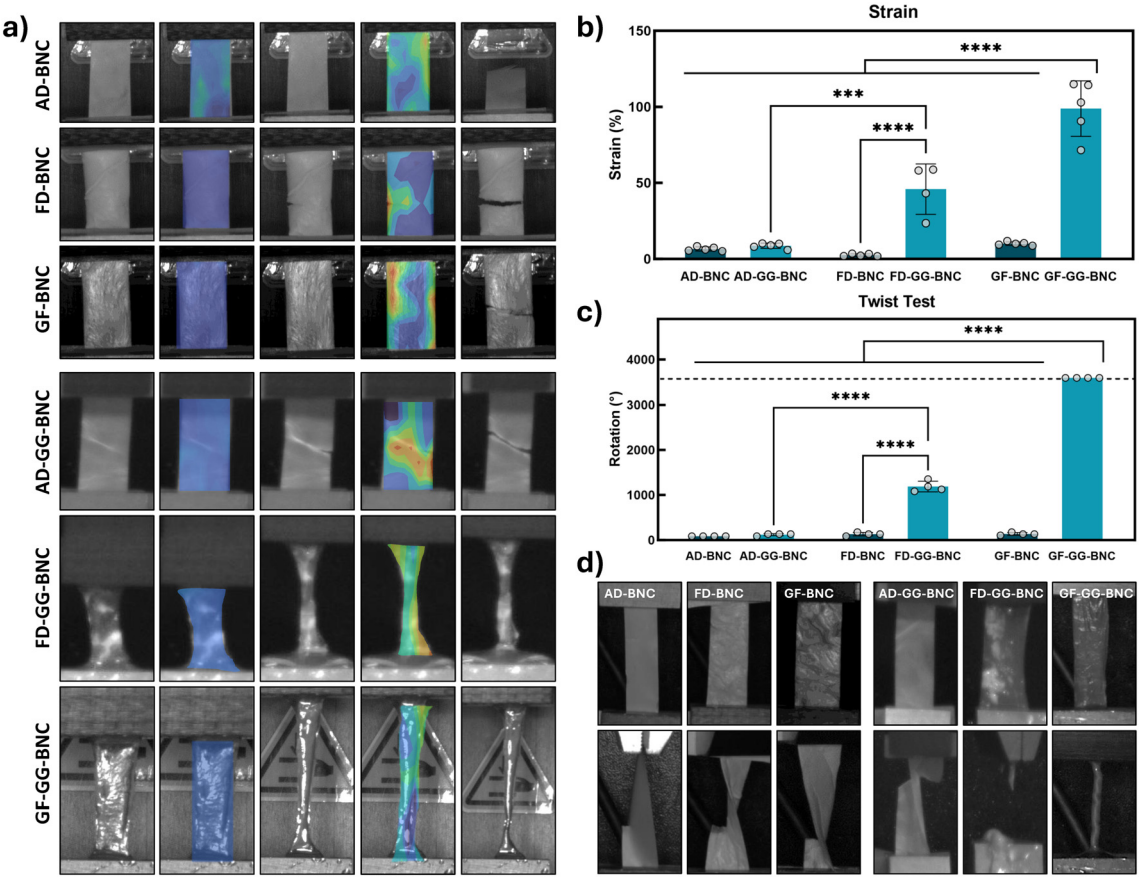

Fig. 3 (a) Images and principal strain mapping of the uniaxial tensile tests. The first and second column of images represent the samples at the beginning of each test when strain is negligible across the sample. The third and fourth columns show the sample immediately prior to rupture, and high levels of strain are indicated with red. The fifth column is post rupture. (b) The strain at rupture for all samples are compared, demonstrating a significant increase in elasticity for both gallic acid/glycerol (GG) loaded FD-GG-BNC and GF-GG-BNC compared to FD-BNC and GF-BNC. The largest strain at rupture is seen in GF-GG-BNC. (c and d) The torsional flexibility of the samples was examined using a twist test, where each sample was subjected to an increasing torsional load until rupture. Images were captured at the beginning of the test (top) and immediately after the sample failed (bottom). All graphs are presented as mean ± standard deviation. $^{****}P \leq 0.0001$, $^{***}P \leq 0.001$, $^{**}P \leq 0.01$.

Table 1 Mechanical properties of dried and drug-loaded BNC materials after performing the uniaxial tensile test. Graphical representation and statistical analysis can be found in ESI Fig. 5†

	AD-BNC	FD-BNC	GF-BNC	AD-GG-BNC	FD-GG-BNC	GF-GG-BNC
UTS (MPa)	22.7 ± 3.9	0.7 ± 0.3	5.6 ± 0.4	55.5 ± 9.3	0.2 ± 0.1	1.2 ± 0.3
Strain at rupture (%)	6.6 ± 1.4	2.6 ± 0.8	10.1 ± 1.2	8.7 ± 1.8	45.9 ± 16.6	98.9 ± 18.3
Young's modulus (MPa)	339.1 ± 97.4	34.4 ± 12.3	60.8 ± 10.8	631.6 ± 79.3	0.4 ± 0.1	1.7 ± 0.6

There are several key contributing factors to the significant decrease in mechanical strength between AD-BNC and FD-BNC. First, as previously discussed, it has been reported that the porosity of a polymer has an inverse relationship with mechanical strength; with the increase in porosity seen in FD-BNC, there are fewer internal bonds and a significant amount of empty space within the material, decreasing its UTS.[80,81] Second, it is hypothesized here that the method in which BNC is frozen to create FD-BNC has a significant effect on its structural integrity. Freezing BNC in a bath of liquid nitrogen is a common method of creating FD-BNC. However, exposing BNC to the extreme cold temperature is theorized to increase its risk of thermal shock. As the water within the pores of the BNC freezes rapidly, it may create both microscopic and macroscopic fractures within the material (Fig. 1b and ESI Fig. 1†), which have a direct impact on its mechanical integrity. The directional alignment of internal cellulose fibers for GF-BNC (Fig. 1c) runs in the same direction as the applied tension in the tensile test; these aligned fibers are hypothesized to directly impact the mechanical integrity of GF-BNC. Materials with fiber alignment in the direction of stress are known to show greater mechanical strength than those with

random alignment.[88–90] This further justifies the significant increase in mechanical strength of GF-BNC when compared to FD-BNC, which has random fiber orientation.

In both FD-GG-BNC and GF-GG-BNC samples, a significant increase in elasticity is evident when compared to their non-GG loaded counterparts (Fig. 3b). Glycerol acts as a plasticizer for polymeric biomaterials;[71,91–93] for this research, samples that have been effectively loaded with GG should demonstrate an increase in elasticity, with some decrease in mechanical strength. When incorporating glycerol into natural polymers, there is a disruption with the intermolecular hydrogen bonds resulting in both an increase in flexibility and decrease in strength of the material.[92,93] When dried, BNC membranes are known to establish varying levels of intermolecular hydrogen bonding,[41] a function of the abundant hydroxyl groups in the material's chemical structure.[94,95] The effects of a plasticizer, such as glycerol, on BNC would therefore interrupt these bonds, resulting in a significant increase in elasticity. While these properties are evident in FD-GG-BNC and GF-GG-BNC samples, the comparison of AD-BNC and AD-GG-BNC demonstrates no such effect. Though there is a small increase in the elasticity of AD-GG-BNC when compared to AD-BNC, this difference is not statistically significant. Additionally, the mechanical strength of AD-GG-BNC is greatly increased, which opposes the expected effect of the glycerol plasticizer. Upon the initial drying procedure, it is reported that the evaporation of water from the cellulosic matrix through air-drying promotes the collapse of the porous microstructure, resulting in a compact and mechanically rigid AD-BNC material.[80] With an increase in mechanical strength after the GG-loading process, which includes a series of water rinses to remove excess GG from the surface of the material, it is hypothesized that there is limited absorption within AD-GG-BNC, and the material instead becomes re-hydrated during the rinsing procedure. This would result in the further compaction of any remaining pores within the material, again increasing its mechanical strength. To confirm this hypothesis, further mechanical tests were performed on AD-BNC membranes that were rehydrated and air-dried a second time, or double-AD-BNC (D-AD-BNC, ESI Fig. 6†). These tests showed that repeating the air-drying process both improved UTS and elasticity of the materials, a behaviour consistent with that of AD-GG-BNC.

To assess resistance to torsional stress, a twist test was performed (Fig. 3c and d). Membranes were clamped into the CellScale UniVert uniaxial testing apparatus and subjected to 1 N of pre-tension. The membranes were then subjected to increasing torsional stress until failure. This test further demonstrates the membranes' flexibility. With each of AD-BNC, FD-BNC and GF-BNC displaying poor tensile elasticity as summarized in Table 1, their failure under small amounts of torsional stress demonstrates further evidence of the general brittleness of dried BNC membranes. In contrast, both FD-GG-BNC and GF-GG-BNC membranes demonstrated favorable elastic behaviour under torsional stress, with all samples of GF-GG-BNC exceeding the limits of the testing apparatus (ten rotations, or 3600°). This is further evidence of successful GG loading in both FD-GG-BNC and GF-GG-BNC, though the torsional elasticity of GF-GG-BNC was significantly greater than that of FD-GG-BNC. The increased torsional elasticity of GF-GG-BNC when compared to FD-GG-BNC, as with tensile elasticity, is hypothesized to be directly related to the stresses placed on FD-BNC during the drying process. As previously mentioned, exposure to extreme cold temperatures during the drying process makes FD-BNC susceptible to fractures. The resulting membranes behave both poorly and unpredictably when subjected to mechanical stresses as fractures within the material are assumed to increase inhomogeneity. Compared to AD-BNC, there was no significant improvement in the torsional elasticity of AD-GG-BNC, indicating that the plasticizing effects of glycerol were not seen in AD-GG-BNC.

With the results demonstrated throughout material characterization and mechanical testing, GF-GG-BNC was determined to be the most optimal material moving forward. SEM images of AD-GG-BNC did not demonstrate any conclusive evidence of GG loading, which was confirmed by the lack of characteristic peaks indicative of glycerol and gallic acid in its ATR-FTIR spectra. Mechanically, the inefficiency in GG loading for AD-GG-BNC was further confirmed as there was no evidence of the plasticizing effects of glycerol in both the tensile and twist tests. Visual evidence of GG loading in FD-GG-BNC samples could be seen with SEM imaging, which was further confirmed with analysis of its ATR-FTIR spectra. While FD-GG-BNC experienced a significant increase in elasticity when compared to FD-BNC, it also demonstrated significantly lower tensile strength than GF-GG-BNC. This can be attributed to the decreased initial mechanical properties of FD-BNC, hypothesized to be caused by thermal stresses during freezing. With these conclusions, the following GG loading and release studies, antibacterial, and blood/plasma interaction studies were conducted using GF-GG-BNC, with GF-BNC as a control material.

Loading and release of GG in GF-BNC

To determine the loading profile of GG into GF-BNC, the change in weight over time of 1 cm × 1 cm samples were monitored (ESI Fig. 2c†). Submerged in GG in normal loading conditions, GF-BNC exhibited rapid GG loading during the initial hours of the test, with sample weight normalizing after 12 hours. In addition, to ensure bulk loading, gallic acid concentration in the GG loading solution was quantified throughout the data collection period. No significant change in gallic acid concertation over time was detected (ESI Fig. 2c†). Rapid uptake of a liquid is characteristic of dried BNC materials; their highly porous nature allows for effective liquid absorption and retention.[5] For GF-BNC, the directional alignment of internal fibers are also suspected to aid in mass transfer, allowing for even viscous solutions such as glycerol to effectively load into the membrane.[76,96]

Over a period of 48 hours, the gallic acid release profile of GF-GG-BNC membranes were characterized using UV-vis spectroscopy (ESI Fig. 2d†). When submerged in PBS at 37 °C,

GF-GG-BNC membranes exhibited a rapid initial release of gallic acid. This release was slowed after 24 hours. The rapid release of gallic acid from GF-GG-BNC membranes shows promise for applications where antibacterial or anticlotting agents must be delivered rapidly, such as at an infection site.

Bacterial adhesion and biofilm formation

To assess the bactericidal properties of GF-GG-BNC membranes, two conventional tests for assessing active antibacterial properties were performed with both *E. coli* and *S. aureus*, which are commonly known to cause severe infections in humans.[97,98] First, the membranes were assessed through a disc diffusion test as described in the materials and methods section.

The zone of inhibition around the samples is indicative of the active antibacterial properties of each of the membranes (Fig. 4a, b and c). GF-BNC demonstrated no active antibacterial properties, and biofilm formation could be seen on the edges of the material. The biofilm formation was further verified *via* SEM, where complex colonies and extracellular polymeric substances were seen for both *E. coli* and *S. aureus* cultures (Fig. 4a, b and c). In contrast, the GF-GG-BNC membranes demonstrated a clear zone of inhibition, and no growth was allowed to occur. This zone demonstrates the ability of gallic acid within the sample to spread to the surrounding area, creating a barrier of protection around the material from both Gram-positive and Gram-negative bacterial strains.[99] Further, SEM imaging of the GF-GG-BNC samples from the disc diffusion test showed no bacteria present on the surface for both bacterial strains, demonstrating its capacity to prevent biofilm formation in the presence of infectious bacteria.

To assess how the control and GG-loaded membranes could affect bacterial growth over time, a bacterial growth curve test was performed (Fig. 4d). Briefly, a suspension of bacteria was prepared in LB media and dispersed into the wells of three 48-well plates with 500 μL of media in each well. GF-BNC and GF-GG-BNC samples were introduced into separate plates, and a third plate was left blank as a negative control. The initial concentration of bacteria was read in the plate reader at 600 nm absorbance at inoculation for each sample with four repeats, and the opacity of the LB media was used as a baseline.[100] Tests were performed over a 24-hour period, with opacity readings at inoculation, 4 hours, 8 hours, 12 hours, and 24 hours to create bacterial growth curves. *S. aureus*

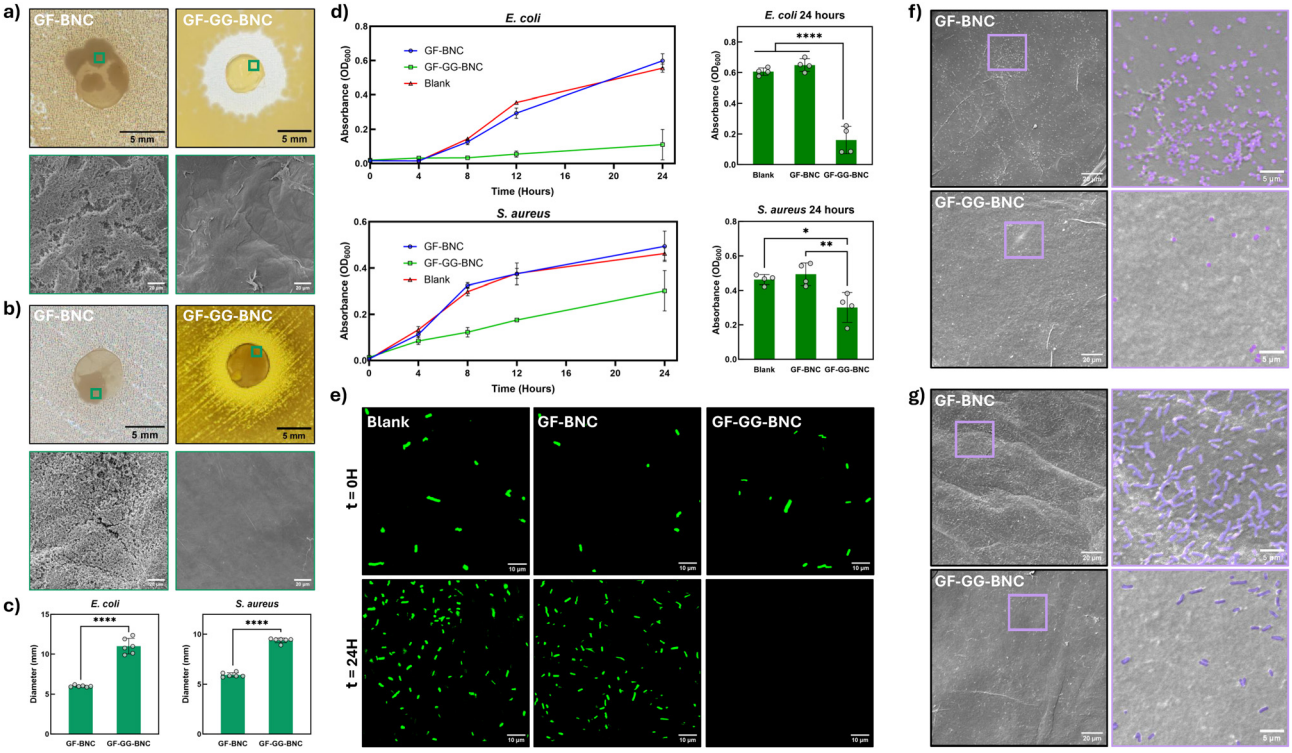

Fig. 4 Disc diffusion tests were performed using both (a) *E. coli* and (b) *S. aureus*, after which samples were preserved for SEM imaging. Comprehensive biofilms were formed on the surface of GF-BNC for both samples, while the GF-GG-BNC samples were devoid of any bacterial adhesion. (c) The zone of inhibition was measured using ImageJ. (d) Bacterial growth throughout the growth curve test was analyzed by detecting the absorbance at 600 nm, with four repeats at each time point. The absorbance after 24 hours demonstrated significant growth inhibition of both *E. coli* and *S. aureus* when compared to controls. (e) GFP-tagged *E. coli* in the wells containing GF-BNC, GF-GG-BNC, and a negative control were fluorescently imaged at inoculation and after 24 hours of incubation for the growth curve test. (f and g) After the test concluded, representative samples were preserved for SEM imaging where an increased number of adhered bacteria could be seen on the surfaces of the GF-BNC samples for both *E. coli* and *S. aureus*. All graphs are reported as mean ± standard deviation. ****$P \leq 0.0001$, **$P \leq 0.01$, *$P \leq 0.05$.

demonstrated a limited growth capacity when GF-GG-BNC membranes were present, while GF-BNC membranes did not significantly change growth when compared to the blank plate. When performed with Gram-negative GFP-tagged *E. coli*, bacterial growth in the presence of GF-GG-BNC was significantly stunted compared to both GF-BNC and the blank plate (Fig. 4e). This indicates that GF-GG-BNC can limit the growth and proliferation of bacteria in an aqueous environment. In addition to opacity readings, fluorescent microscopy was performed for the samples incubated with GFP-tagged *E. coli.* Immediately after inoculation, fluorescent images of the media from each test group indicated even inoculation across all sample groups (Fig. 4e). At 24 hours, there was no evident fluorescence remaining in the media exposed to GF-GG-BNC. An increased number of bacteria were seen when GF-BNC was present, as well as in the blank well. GFP-tagging provides a unique insight for this experiment as a live-cell fluorescent indicator;[101,102] with the *E. coli* exposed to GF-GG-BNC samples demonstrating no evidence of fluorescence after 24 hours, it can be concluded that the bacteria were not just prevented from proliferating but were not able to survive in their environment. For the experiments conducted with both *S. aureus* and GFP-tagged *E. coli*, representative samples were imaged using SEM to detect bacterial adhesion on their surfaces, where it was seen that GF-BNC had significantly more bacterial adhesion than the GF-GG-BNC membranes when exposed to both strains (Fig. 4f and g).

Gallic acid is a known antibacterial agent.[97,103] With the ability to penetrate bacterial cell walls, gallic acid kills bacteria by damaging genetic material and causing oxidative stress.[104] Additionally, gallic acid has been observed to promote pore formation in the bacterial membrane, which alters membrane permeability and limits the controlled transfer of substances.[60,104,105] In addition to its innate antibacterial activities, gallic acid is known to both prevent biofilm formation and disrupt existing biofilms.[97] Biofilm infections are known to be particularly difficult to treat. Bacteria in biofilms behave differently than planktonic bacteria; the extracellular polymeric substances secreted by biofilm-forming bacteria act as a barrier for the contained colonies, preventing effective treatment with antibiotics.[106,107] A recent study suggests that gallic acid prevents biofilm formation by decreasing the adhesion capacity of biofilm-forming bacteria.[97] This explanation is consistent with the results displayed in Fig. 4f and g, where bacterial adhesion to the surface of GF-GG-BNC is significantly decreased compared to GF-BNC.

Blood and plasma interactions

Blood and plasma interactions should be evaluated for biomaterials, especially those intended for blood-contacting applications. The time-to-clot was assessed visually for plasma exposed to GF-BNC, GF-G-BNC, and GF-GG-BNC samples and in a blank well as a negative control. To allow for sufficient visualization of clotting, the samples were cut into strips and placed along the walls of a 48-well plate. The plates were agitated on a plate shaker and incubated at 37 °C throughout the experiment. Human plasma exposed to GF-BNC showed significant clotting after just four minutes, with a clot mass firmly adhered to the surface of the samples (Fig. 5a). GF-G-BNC demonstrated the ability to slightly attenuate clotting, as clot masses could be visualized after six minutes. In contrast, the plasma exposed to GF-GG-BNC samples lacked any significant clot mass either attached to the sample or in the well even after four hours of incubation, at which the experiment was concluded. SEM imaging confirmed cohesive clotting on the surface of GF-BNC and GF-G-BNC samples. In contrast, small fibrous aggregates could be seen on the surface of GF-GG-BNC, though no cohesive clotting was visually identified.

Red blood cell adhesion on the surface of the membranes was assessed as previously described.[108] As shown in Fig. 5b, circular samples cut with an 8 mm biopsy punch were incubated in 500 μL of citrated whole blood for 45 s. The samples were then quickly removed from the blood, and non-adhered blood was taken from the surface of the sample by tapping it gently on a piece of paper towel. To release adhered blood cells from the surface of the samples, they were placed in 700 μL of distilled water and agitated at 240 rpm for 45 minutes. To quantify the released blood cells in the distilled water, 200 μL of solution from each well was transferred to a 96-well plate and the absorbance at 450 nm was recorded. As shown in Fig. 5b, GF-G-BNC and GF-GG-BNC samples demonstrated reduced red blood cell adhesion when compared to GF-BNC.

The coagulation cascade is a complex physiological pathway leading to thrombus formation. Studies have shown that gallic acid could interact with the coagulation cascade through two pathways. The primary method of interaction, and the most prominent in the described plasma clotting protocol, is as a direct thrombin inhibitor.[109] In the coagulation cascade, thrombin converts fibrinogen into fibrin, forming a clot mesh.[110,111] In acting as a thrombin inhibitor, gallic acid prevents clotting through a similar mechanism to heparin. By binding to one of several common binding sites on thrombin, gallic acid has both previously and, in this work, demonstrated significant antithrombotic effects.[109] Gallic acid is also known to limit platelet activation, demonstrating potential as a vascular health therapeutic for those at risk of vascular occlusion.[112]

While the effects of gallic acid and glycerol on red blood cell adhesion have only been limitedly studied, the reasons for a significant decrease in red blood cell adhesion to the surface may be attributed to (a) how phenolic acids interact with blood proteins, and (b) how glycerol limits protein aggregation. In citrated whole blood, red blood cells can adhere to a surface through adsorbed proteins on a materials surface, such as fibrinogen, albumin, and von Willebrand factor.[113] In one previous study, tannic acid was found to change the morphology of fibrinogen in whole blood, preventing effective blood adhesion and transformation to fibrin within the coagulation cascade.[114] Tannic acid is a phenolic acid which includes a gallic acid unit and is known to have many of the same properties;[115] with this, it can be hypothesized that gallic acid may have the same effects as tannic acid on fibrinogen. In a

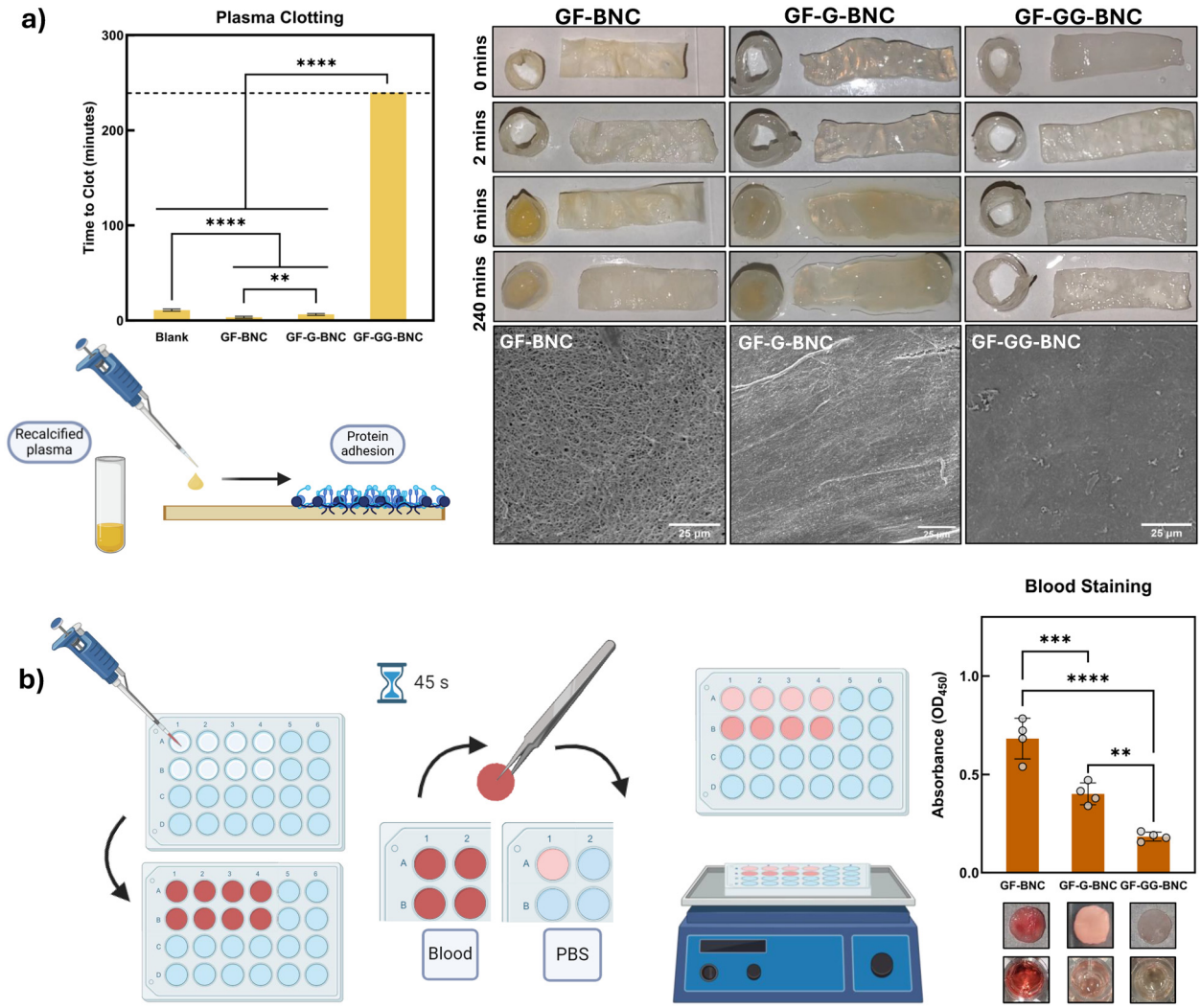

Fig. 5 (a) A plasma clotting assay was performed over a period of four hours. Clot formation was seen on gradually-frozen BNC (GF-BNC) and gradually-frozen glycerol loaded BNC (GF-G-BNC) samples after four and six minutes of incubation respectively. In contrast, gradually-frozen gallic acid/glycerol loaded BNC (GF-GG-BNC) samples did not show visible clotting even after four hours and a clotting time of 4 hours was assigned to these samples. Samples were fixed after four hours for SEM imaging. A fibrin clot network was evident on the surface of the GF-BNC and GF-G-BNC samples, while no visible clot formation was observed on the GF-GG-BNC samples. Schematic created in BioRender. E. Stephens (2025). https://BioRender.com/9qq89vd. (b) The procedure as followed for conducting the blood staining test. Blood staining was evaluated for GF-BNC, GF-G-BNC and GF-GG-BNC samples by measuring absorbance using a plate reader at 450 nm. Schematic created in BioRender. E. Stephens (2025). https://BioRender.com/o66zskq. All graphs are reported as mean ± standard deviation. $^{****}P \leq 0.0001$, $^{***}P \leq 0.001$, $^{**}P \leq 0.01$.

dual-acting perspective, glycerol has also been indicated as having adhesion-reducing effects on proteins. When interacting with water, as found in blood, glycerol released from the membranes may compact proteins as it is released from the material and seeks a favorable electrostatic orientation.[116] While GF-G-BNC did demonstrate improved plasma clotting and red blood cell adhesion properties when compared to GF-BNC, the combination of gallic acid and glycerol in GF-GG-BNC has demonstrated a stronger ability to decrease red blood cell adhesion. When taken in conjunction with the material's anticoagulant effects, these results demonstrate GF-GG-BNC is a promising material for blood contacting applications.

Conclusion

Unlike traditional air-drying and freeze-drying methods, GF-BNC membranes present a material option with tunable mechanical properties without sacrificing microstructural properties that are key in promoting biological interactions and drug loading. The balance between mechanical strength and aligned porous morphology as seen in GF-BNC addresses the microstructural compaction seen in AD-BNC and the unfavorable behavior under stress of FD-BNC, and the successful integration of gallic acid as an antifouling agent makes clear that GF-BNC is a strong candidate for drug loading and delivery. The successful loading of gallic acid into BNC membranes pro-

duced a material with antibacterial and antithrombotic properties, while significantly increasing the elasticity of the BNC materials by using glycerol as a solvent and plasticizer. The resulting optimized material, GF-GG-BNC, demonstrated comprehensive material properties including consistent mechanical strength with tissue-like elasticity, bactericidal effects on both Gram-negative *E. coli* and Gram-positive *S. aureus*, and antithrombotic effects when exposed to blood plasma. GF-GG-BNC has significant applicability for blood-contacting and antimicrobial applications, such as for wound dressings. Further studies may investigate alternative freezing rates and final temperatures for BNC membranes, as this may allow for the mechanical and microstructural properties of the membrane to be tuned for more specific applications. In addition, *in vivo* biocompatibility studies of both GF-BNC and GF-GG-BNC would provide a better understanding of the clinical practicality of both directionally aligned BNC material and GG as an antithrombotic and antibacterial agent. Overall, both GF-BNC and gallic acid-loaded materials show strong promise in the future of biomaterials and biomedical engineering, with general applicability for blood-contacting and antimicrobial applications.

Author contributions

E. D. S. designed and performed the experiments, analyzed the data, and wrote the manuscript. F. O. assisted with the blood staining and plasma clotting experiments. H. M. performed the AFM testing under P. E. supervision. J. L. V. assisted with the bacterial adhesion studies. K. M. provided the equipment and experimental guidelines for the freezing studies. M. B. conceived and conceptualized the project, supervised the experiments, and provided guidance throughout the experimental design process, data analysis, and manuscript writing. All authors have reviewed and edited the manuscript and approved the final submission.

Data availability

The authors confirm that the data supporting the findings of this study are available within the article and/or in the ESI.†

Conflicts of interest

The authors declare no conflict of interest.

Acknowledgements

This work was supported by University of Calgary start-up funds and NSERC Alliance – Alberta Innovates Advance Program, Stream I (no. RMS22-96817842-1) awarded to M. B.

References

1 P. Jacek, M. Ryngajłło and S. Bielecki, Structural changes of bacterial nanocellulose pellicles induced by genetic modification of Komagataeibacter hansenii ATCC 23769, *Appl. Microbiol. Biotechnol.*, 2019, **103**(13), 5339–5353.
2 I. Cielecka, M. Ryngajłło, W. Maniukiewicz and S. Bielecki, Highly Stretchable Bacterial Cellulose Produced by Komagataeibacter hansenii SI1, *Polymers*, 2021, **13**(24), 4455.
3 B. V. Mohite and S. V. Patil, Physical, structural, mechanical and thermal characterization of bacterial cellulose by G. hansenii NCIM 2529, *Carbohydr. Polym.*, 2014, **106**, 132–141.
4 P. Jacek, K. Kubiak, M. Ryngajłło, P. Rytczak, P. Paluch and S. Bielecki, Modification of bacterial nanocellulose properties through mutation of motility related genes in Komagataeibacter hansenii ATCC 53582, *New Biotechnol.*, 2019, **52**, 60–68.
5 F. Barja, Bacterial nanocellulose production and biomedical applications, *J. Biomed. Res.*, 2021, **35**(4), 310.
6 E. L. Roberts, S. Abdollahi, F. Oustadi, E. D. Stephens and M. Badv, Bacterial-Nanocellulose-Based Biointerfaces and Biomimetic Constructs for Blood-Contacting Medical Applications, *ACS Mater. Au*, 2023, **3**(5), 418–441.
7 S. Fooladi, M. H. Nematollahi, N. Rabiee and S. Iravani, Bacterial Cellulose-Based Materials: A Perspective on Cardiovascular Tissue Engineering Applications, *ACS Biomater. Sci. Eng.*, 2023, **9**(6), 2949–2969.
8 A. Zarepour, B. Gok, Y. Budama-Kilinc, A. Khosravi, S. Iravani and A. Zarrabi, Bacterial nanocelluloses as sustainable biomaterials for advanced wound healing and dressings, *J. Mater. Chem. B*, 2024, **12**(48), 12489–12507.
9 K. Malekpour, A. Hazrati, A. Khosrojerdi, L. Roshangar and M. Ahmadi, An overview to nanocellulose clinical application: Biocompatibility and opportunities in disease treatment, *Regen. Ther.*, 2023, **24**, 630–641.
10 A. Kumar and S. S. Han, Efficacy of Bacterial Nanocellulose in Hard Tissue Regeneration: A Review, *Materials*, 2021, **14**(17), 4777.
11 V. Potočnik, S. Gorgieva and J. Trček, From Nature to Lab: Sustainable Bacterial Cellulose Production and Modification with Synthetic Biology, *Polymers*, 2023, **15**(16), 3466.
12 P. P. Acharyya, M. Sarma and A. Kashyap, Recent advances in synthesis and bioengineering of bacterial nanocellulose composite films for green, active and intelligent food packaging, *Cellulose*, 2024, **31**(12), 7163–7187.
13 J. Cattelaens, L. Turco, L. M. Berclaz, B. Huelsse, W. Hitzl, T. Vollkommer, *et al.*, The Impact of a Nanocellulose-Based Wound Dressing in the Management of Thermal Injuries in Children: Results of a Retrospective Evaluation, *Life*, 2020, **10**(9), 212.
14 M. Shahriari-Khalaji, S. Hong, G. Hu, Y. Ji and F. F. Hong, Bacterial Nanocellulose-Enhanced Alginate Double-Network Hydrogels Cross-Linked with Six Metal Cations

for Antibacterial Wound Dressing, *Polymers*, 2020, **12**(11), 2683.

15 A. Müller, M. Zink, N. Hessler, F. Wesarg, F. A. Müller, D. Kralisch, *et al.*, Bacterial nanocellulose with a shape-memory effect as potential drug delivery system, *RSC Adv.*, 2014, **4**(100), 57173–57184.

16 G. N. Balistreri, I. R. Campbell, X. Li, J. Amorim, S. Zhang, E. Nance, *et al.*, Bacterial cellulose nanoparticles as a sustainable drug delivery platform for protein-based therapeutics, *RSC Appl. Polym.*, 2024, **2**(2), 172–183.

17 N. H. C. S. Silva, J. P. Mota, T. S. Almeida, J. P. F. Carvalho, A. J. D. Silvestre, C. Vilela, *et al.*, Topical Drug Delivery Systems Based on Bacterial Nanocellulose: Accelerated Stability Testing, *Int. J. Mol. Sci.*, 2020, **21**(4), 1262.

18 S. Adepu and M. Khandelwal, Ex-situ modification of bacterial cellulose for immediate and sustained drug release with insights into release mechanism, *Carbohydr. Polym.*, 2020, **249**, 116816.

19 L. Bao, F. F. Hong, G. Li, G. Hu and L. Chen, Improved Performance of Bacterial Nanocellulose Conduits by the Introduction of Silk Fibroin Nanoparticles and Heparin for Small-Caliber Vascular Graft Applications, *Biomacromolecules*, 2021, **22**(2), 353–364.

20 D. Liu, Q. Meng and J. Hu, Bacterial Nanocellulose Hydrogel: A Promising Alternative Material for the Fabrication of Engineered Vascular Grafts, *Polymers*, 2023, **15**(18), 3812.

21 C. Molina-Ramírez, J. Álvarez, R. Zuluaga, C. Castro and P. Gañán, A Novel Approach Using Conventional Methodologies to Scale up BNC Production Using Komagataeibacter medellinensis and Rotten Banana Waste as Alternative, *Processes*, 2020, **8**(11), 1469.

22 D. Abol-Fotouh, M. A. Hassan, H. Shokry, A. Roig, M. S. Azab and A. E. H. B. Kashyout, Bacterial nanocellulose from agro-industrial wastes: low-cost and enhanced production by Komagataeibacter saccharivorans MD1, *Sci. Rep.*, 2020, **10**(1), 3491.

23 N. A. Shavyrkina, V. V. Budaeva, E. A. Skiba, G. F. Mironova, N. V. Bychin, Y. A. Gismatulina, *et al.*, Scale-Up of Biosynthesis Process of Bacterial Nanocellulose, *Polymers*, 2021, **13**(12), 1920.

24 I. S. Mir, A. Riaz, J. Fréchette, J. S. Roy, J. Mcelhinney, S. Pu, *et al.*, Bacterial cellulose-graphene oxide composite membranes with enhanced fouling resistance for bio-effluents management, *Npj Clean Water*, 2024, **7**(1), 111.

25 K. Ludwicka, M. Kaczmarek and A. Białkowska, Bacterial Nanocellulose—A Biobased Polymer for Active and Intelligent Food Packaging Applications: Recent Advances and Developments, *Polymers*, 2020, **12**(10), 2209.

26 S. Abdollahi, E. D. Stephens, M. A. Uy, A. Fatehi Hassanabad, P. W. M. Fedak and M. Badv, Super-Repellent and Flexible Lubricant-Infused Bacterial Nanocellulose Membranes with Superior Antithrombotic, Antibacterial, and Fatigue Resistance Properties, *ACS Appl. Mater. Interfaces*, 2023, **15**(22), 26417–26430.

27 T. V. Patil, D. K. Patel, S. D. Dutta, K. Ganguly, T. S. Santra and K. T. Lim, Nanocellulose, a versatile platform: From the delivery of active molecules to tissue engineering applications, *Bioact. Mater.*, 2022, **9**, 566–589.

28 S. C. De Assis, D. L. Morgado, D. T. Scheidt, S. S. De Souza, M. R. Cavallari, O. H. Ando Junior, *et al.*, Review of Bacterial Nanocellulose-Based Electrochemical Biosensors: Functionalization, Challenges, and Future Perspectives, *Biosensors*, 2023, **13**(1), 142.

29 A. Stanisławska, M. Szkodo, H. Staroszczyk, K. Dawidowska, M. Kołaczkowska and P. Siondalski, Effect of the ex situ physical and in situ chemical modification of bacterial nanocellulose on mechanical properties in the context of its potential applications in heart valve design, *Int. J. Biol. Macromol.*, 2024, **269**, 131951.

30 I. Betlej, R. Salerno-Kochan, A. Jankowska, K. Krajewski, J. Wilkowski, K. Rybak, *et al.*, The Impact of the Mechanical Modification of Bacterial Cellulose Films on Selected Quality Parameters, *Coatings*, 2021, **11**(11), 1275.

31 G. Zhang, G. Chen, M. Dong, J. Nie and G. Ma, Multifunctional Bacterial Cellulose/Covalent Organic Framework Composite Membranes with Antifouling and Antibacterial Properties for Dye Separation, *ACS Appl. Mater. Interfaces*, 2023, **15**(27), 32903–32915.

32 L. Li, G. Li, Y. Wu, Y. Lin, Y. Qu, Y. Wu, *et al.*, Dual-functional bacterial cellulose modified with phase-transitioned proteins and gold nanorods combining antifouling and photothermal bactericidal properties, *J. Mater. Sci. Technol.*, 2022, **110**, 14–23.

33 M. Imanbekova, R. Abbasi, X. Hu, M. Sharma, M. Vandewynckele-Bossut, R. Haldavnekar, *et al.*, Physical Modifications of Kombucha–Derived Bacterial Nanocellulose: Toward a Functional Bionanocomposite Platform, *Macromol. Mater. Eng.*, 2024, **309**(10), 2400041.

34 R. Reshmy, E. Philip, D. Thomas, A. Madhavan, R. Sindhu, P. Binod, *et al.*, Bacterial nanocellulose: engineering, production, and applications, *Bioengineered*, 2021, **12**(2), 11463–11483.

35 R. Prathapan, A. K. Ghosh, A. Knapp, A. Vijayakumar, N. N. J. Bogari, B. D. Abraham, *et al.*, *In Situ* Alignment of Bacterial Cellulose Using Wrinkling, *ACS Appl. Bio Mater.*, 2020, **3**(11), 7898–7907.

36 F. Wahid, X. J. Zhao, X. Q. Zhao, X. F. Ma, N. Xue, X. Z. Liu, *et al.*, Fabrication of Bacterial Cellulose-Based Dressings for Promoting Infected Wound Healing, *ACS Appl. Mater. Interfaces*, 2021, **13**(28), 32716–32728.

37 W. He, J. Wu, J. Xu, D. A. Mosselhy, Y. Zheng and S. Yang, Bacterial Cellulose: Functional Modification and Wound Healing Applications, *Adv. Wound Care*, 2021, **10**(11), 623–640.

38 M. Horue, J. M. Silva, I. R. Berti, L. R. Brandão, H. D. S. Barud and G. R. Castro, Bacterial Cellulose-Based Materials as Dressings for Wound Healing, *Pharmaceutics*, 2023, **15**(2), 424.

39 N. T. P. Nguyen, H. H. Nguyen, H. N. Doan, K. T. Pham, K. Van Nguyen, B. T. Vu, *et al.*, Chitosan oligosaccharide-

loaded bacterial cellulose membrane for hemostatic dressing, *Cellulose*, 2023, **30**(18), 11649–11664.

40 I. Orlando, P. Basnett, R. Nigmatullin, W. Wang, J. C. Knowles and I. Roy, Chemical Modification of Bacterial Cellulose for the Development of an Antibacterial Wound Dressing, *Front. Bioeng. Biotechnol.*, 2020, **8**, 557885.

41 V. Andree, D. Niopek, C. Müller, J. P. Eiselt, N. Foh, A. Rzany, *et al.*, Influence of drying methods on the physical properties of bacterial nanocellulose, *Mater. Res. Express*, 2021, **8**(2), 025402.

42 M. P. Illa, C. S. Sharma and M. Khandelwal, Tuning the physiochemical properties of bacterial cellulose: effect of drying conditions, *J. Mater. Sci.*, 2019, **54**(18), 12024–12035.

43 S. Sozcu, J. Frajova, J. Wiener, M. Venkataraman, B. Tomkova and J. Militky, Effect of Drying Methods on the Thermal and Mechanical Behavior of Bacterial Cellulose Aerogel, *Gels*, 2024, **10**(7), 474.

44 M. Farzan, R. Roth, J. Schoelkopf, J. Huwyler and M. Puchkov, The processes behind drug loading and release in porous drug delivery systems, *Eur. J. Pharm. Biopharm.*, 2023, **189**, 133–151.

45 G. M. Raghavendra, K. Varaprasad and T. Jayaramudu, Biomaterials, in *Nanotechnology Applications for Tissue Engineering [Internet]*, Elsevier, 2015, pp. 21–44. Available from: **https://linkinghub.elsevier.com/retrieve/pii/B9780323328890000029**, (accessed January 2025).

46 M. N. F. Norrrahim, N. M. Nurazzi, M. A. Jenol, M. A. A. Farid, N. Janudin, F. A. Ujang, *et al.*, Emerging development of nanocellulose as an antimicrobial material: an overview, *Mater. Adv.*, 2021, **2**(11), 3538–3551.

47 H. Ao and X. Xun, Bacterial Nanocellulose: Methods, Properties, and Biomedical Applications, in *Nanotechnology and Nanomaterials [Internet]*, ed. Md Salim Newaz Kazi, IntechOpen, 2024, Available from: **https://www.intechopen.com/chapters/89096**, (accessed January 2025).

48 R. Koski, *Medications Associated With Implantable Cardiac Devices*, US Pharm., 2016, vol. 42((2)), pp. 30–34.

49 Antimicrobial Resistance in Health Care: Causes and How It Spreads [Internet]. Center for Disease Control. 2024. Available from: **https://www.cdc.gov/antimicrobial-resistance/causes/healthcare.html**, (accessed January 2025).

50 R. A. Weinstein, Controlling Antimicrobial Resistance in Hospitals: Infection Control and Use of Antibiotics, *Emerging Infect. Dis.*, 2001, **7**(2), 188–192.

51 A. Subramanian, Emerging roles of bacteriophage-based therapeutics in combating antibiotic resistance, *Front. Microbiol.*, 2024, **15**, 1384164.

52 M. Łusiak-Szelachowska, R. Międzybrodzki, Z. Drulis-Kawa, K. Cater, P. Knežević, C. Winogradow, *et al.*, Bacteriophages and antibiotic interactions in clinical practice: what we have learned so far, *J. Biomed. Sci.*, 2022, **29**(1), 23.

53 M. Terreni, M. Taccani and M. Pregnolato, New Antibiotics for Multidrug-Resistant Bacterial Strains: Latest Research Developments and Future Perspectives, *Molecules*, 2021, **26**(9), 2671.

54 K. J. Y. Wu, B. I. C. Tresco, A. Ramkissoon, E. V. Aleksandrova, E. A. Syroegin, D. N. Y. See, *et al.*, An antibiotic preorganized for ribosomal binding overcomes antimicrobial resistance, *Science*, 2024, **383**(6684), 721–726.

55 J. Aparicio-Blanco, I. I. López-Torres, M. Alonso-Berenguel, A. I. Torres-Suárez and C. Martín-Sabroso, Local antimicrobial delivery systems for prophylaxis and treatment of periprosthetic traumatological infections, *Eur. J. Pharm. Sci.*, 2025, **204**, 106940.

56 J. Sliepen, R. A. Corrigan, M. Dudareva, M. Wouthuyzen-Bakker, R. J. Rentenaar, B. L. Atkins, *et al.*, Does the Use of Local Antibiotics Affect Clinical Outcome of Patients with Fracture-Related Infection?, *Antibiotics*, 2022, **11**(10), 1330.

57 B. Bahramian, R. Abedi-Firoozjah, N. Kiani-Salmi, A. Azizian, N. Dorud, S. M. A. Noori, *et al.*, Multifunctional performance of gallic acid in biodegradable food packaging films and coatings: Mechanisms, developments, applications, and horizons, *Eur. Polym. J.*, 2024, **221**, 113559.

58 Z. Xiang, H. Guan, X. Zhao, Q. Xie, Z. Xie, F. Cai, *et al.*, Dietary gallic acid as an antioxidant: A review of its food industry applications, health benefits, bioavailability, nano-delivery systems, and drug interactions, *Food Res. Int.*, 2024, **180**, 114068.

59 M. Ashrafizadeh, A. Zarrabi, S. Mirzaei, F. Hashemi, S. Samarghandian, A. Zabolian, *et al.*, Gallic acid for cancer therapy: Molecular mechanisms and boosting efficacy by nanoscopical delivery, *Food Chem. Toxicol.*, 2021, **157**, 112576.

60 S. Keyvani-Ghamsari, M. Rahimi and K. Khorsandi, An update on the potential mechanism of gallic acid as an antibacterial and anticancer agent, *Food Sci. Nutr.*, 2023, **11**(10), 5856–5872.

61 M. Bhuia, M. Rahaman, T. Islam, M. H. Bappi, M. Sikder, K. N. Hossain, *et al.*, Neurobiological effects of gallic acid: current perspectives, *Chin. Med.*, 2023, **18**(1), 27.

62 Y. Zhang, X. Wang, B. Lu, Y. Gao, Y. Zhang, Y. Li, *et al.*, Functional and binding studies of gallic acid showing platelet aggregation inhibitory effect as a thrombin inhibitor, *Chin. Herb. Med.*, 2022, **14**(2), 303–309.

63 S. R. K. Sah, M. S. Al Hasan, L. K. Thakur, M. Shadin, R. Chowdhury, S. Ahammed, *et al.*, Assessment of clot-lysing and membrane-stabilizing activity of gallic acid through cyclooxygenase-1 and plasminogen interaction pathways, *Food Biosci.*, 2025, **63**, 105673.

64 B. Kang, T. Vales, B. K. Cho, J. K. Kim and H. J. Kim, Development of Gallic Acid-Modified Hydrogels Using Interpenetrating Chitosan Network and Evaluation of Their Antioxidant Activity, *Molecules*, 2017, **22**(11), 1976.

65 R. Cassano, F. Curcio, R. Sole, S. Mellace and S. Trombino, Gallic Acid-Based Hydrogels for Phloretin Intestinal Release: A Promising Strategy to Reduce Oxidative Stress in Chronic Diabetes, *Molecules*, 2024, **29**(5), 929.

66 I. Zarandona, A. I. Puertas, M. T. Dueñas, P. Guerrero and K. De La Caba, Assessment of active chitosan films incorporated with gallic acid, *Food Hydrocolloids*, 2020, **101**, 105486.

67 W. Gong, R. Wang, H. Huang, Y. Hou, X. Wang, W. He, *et al.*, Construction of double network hydrogels using agarose and gallic acid with antibacterial and anti-inflammatory properties for wound healing, *Int. J. Biol. Macromol.*, 2023, **227**, 698–710.

68 A. Naeem, C. Yu, W. Zhu, X. Chen, X. Wu, L. Chen, *et al.*, Gallic Acid-Loaded Sodium Alginate-Based (Polyvinyl Alcohol-Co-Acrylic Acid) Hydrogel Membranes for Cutaneous Wound Healing: Synthesis and Characterization, *Molecules*, 2022, **27**(23), 8397.

69 N. Kahkeshani, F. Farzaei, M. Fotouhi, S. S. Alavi, R. Bahramsoltani, R. Naseri, *et al.*, Pharmacological effects of gallic acid in health and disease: A mechanistic review, *Iran. J. Basic Med. Sci.*, 2019, **22**(3), 225–237.

70 National Library of Medicine (PubChem) [Internet]. Gallic Acid (Compound). Available from:**https://pubchem.ncbi.nlm.nih.gov/compound/Gallic-Acid**, (accessed January 2025).

71 J. Tarique, S. M. Sapuan and A. Khalina, Effect of glycerol plasticizer loading on the physical, mechanical, thermal, and barrier properties of arrowroot (Maranta arundinacea) starch biopolymers, *Sci. Rep.*, 2021, **11**(1), 13900.

72 S. N. Fauziyah, A. S. Mubarak and D. Y. Pujiastuti, Application of glycerol on bioplastic based carrageenan waste cellulose on biodegradability and mechanical properties bioplastic, *IOP Conf. Ser.: Earth Environ. Sci.*, 2021, **679**(1), 012005.

73 J. W. Yau, A. R. Stafford, P. Liao, J. C. Fredenburgh, R. Roberts and J. I. Weitz, Mechanism of catheter thrombosis: comparison of the antithrombotic activities of fondaparinux, enoxaparin, and heparin in vitro and in vivo, *Blood*, 2011, **118**(25), 6667–6674.

74 D. Nečas and P. Klapetek, Gwyddion: an open-source software for SPM data analysis, *Open Phys.*, 2012, **10**(1), 181–188.

75 A. Stylianou, V. Gkretsi, C. S. Patrickios and T. Stylianopoulos, Exploring the nano-surface of collagenous and other fibrotic tissues with AFM, *Fibrosis*, 2017, 453–459.

76 M. A. Shahbazi, M. Ghalkhani and H. Maleki, Directional Freeze–Casting: A Bioinspired Method to Assemble Multifunctional Aligned Porous Structures for Advanced Applications, *Adv. Eng. Mater.*, 2020, **22**(7), 2000033.

77 H. Bai, Y. Chen, B. Delattre, A. P. Tomsia and R. O. Ritchie, Bioinspired large-scale aligned porous materials assembled with dual temperature gradients, *Sci. Adv.*, 2015, **1**(11), e1500849.

78 Q. Sun, R. Tan, Y. Yan, S. Wang, S. Fu, S. Zheng, *et al.*, Production of High-Value-Added Bacterial Nanocellulose with Thinner Fiber Using Novel *Yarrowia lipolytica* Extract from Erythritol Industry Waste, *ACS Sustainable Chem. Eng.*, 2024, **12**(9), 3450–3460.

79 L. Staňková, A. Kutová, M. Doubková, O. Kvítek, B. Vokatá, A. Sedlář, *et al.*, Argon plasma-modified bacterial nanocellulose: Cell-specific differences in the interaction with fibroblasts and endothelial cells, *Carbohydr. Polym. Technol. Appl.*, 2024, **7**, 100470.

80 A. Stanisławska, H. Staroszczyk and M. Szkodo, The effect of dehydration/rehydration of bacterial nanocellulose on its tensile strength and physicochemical properties, *Carbohydr. Polym.*, 2020, **236**, 116023.

81 C. Jantarat, P. Muenraya, S. Srivaro, A. Nawakitrangsan and K. Promsornpason, Comparison of drug release behavior of bacterial cellulose loaded with ibuprofen and propranolol hydrochloride, *RSC Adv.*, 2021, **11**(59), 37354–37365.

82 N. Tamura, K. Hasunuma, T. Saito and S. Fujisawa, Mechanical and Thermal Properties of Porous Nanocellulose/Polymer Composites: Influence of the Polymer Chemical Structure and Porosity, *ACS Omega*, 2024, **9**(17), 19560–19565.

83 L. Solhi, V. Guccini, K. Heise, I. Solala, E. Niinivaara, W. Xu, *et al.*, Understanding Nanocellulose–Water Interactions: Turning a Detriment into an Asset, *Chem. Rev.*, 2023, **123**(5), 1925–2015.

84 M. Kačuráková, A. C. Smith, M. J. Gidley and R. H. Wilson, Molecular interactions in bacterial cellulose composites studied by 1D FT-IR and dynamic 2D FT-IR spectroscopy, *Carbohydr. Res.*, 2002, **337**(12), 1145–1153.

85 M. M. Fathy, A. A. Elfiky, Y. S. Bashandy, M. M. Hamdy, A. M. Elgharib, I. M. Ibrahim, *et al.*, An insight into synthesis and antitumor activity of citrate and gallate stabilizing gold nanospheres, *Sci. Rep.*, 2023, **13**(1), 2749.

86 M. Danish and U. Rashid, Response Surface Methodology based Optimized Purification of the Residual Glycerol from Biodiesel Production Process, *Chiang Mai J. Sci.*, 2017, **44**(4), 1570–1582.

87 D. A. Patil, V. E. Naiker, G. A. Phalak, A. P. More and S. T. Mhaske, Synthesis of benzoxazine from eugenol and its co-polymerization with a gallic acid-based epoxy resin for flame retardant application, *Polym. Bull.*, 2024, **81**(8), 7441–7465.

88 H. V. Patel and H. K. Dave, Effect of fiber orientation on tensile strength of thin composites, *Mater. Today: Proc.*, 2021, **46**, 8634–8638.

89 H. M. Ananzeh, R. Ramli, S. Julai and A. G. A. Muthalif, Mechanical Properties Comparison of Isotropic vs. Anisotropic Hybrid Magnetorheological Elastomer-Fluid, *Polymers*, 2024, **16**(9), 1215.

90 D. McNally, Short Fiber orientation and its Effects on the Properties of Thermoplastic Composite Materials, *Polym.-Plast. Technol. Eng.*, 1977, **8**(2), 101–154.

91 C. Gao, E. Pollet and L. Avérous, Properties of glycerol-plasticized alginate films obtained by thermo-mechanical mixing, *Food Hydrocolloids*, 2017, **63**, 414–420.
92 Z. Eslami, S. Elkoun, M. Robert and K. Adjallé, A Review of the Effect of Plasticizers on the Physical and Mechanical Properties of Alginate-Based Films, *Molecules*, 2023, **28**(18), 6637.
93 J. J. Benitez, P. Florido-Moreno, J. M. Porras-Vázquez, G. Tedeschi, A. Athanassiou, J. A. Heredia-Guerrero, *et al.*, Transparent, plasticized cellulose-glycerol bioplastics for food packaging applications, *Int. J. Biol. Macromol.*, 2024, **273**, 132956.
94 D. M. Sánchez-Osorno, D. Gomez-Maldonado, C. Castro and M. S. Peresin, Surface Interactions between Bacterial Nanocellulose and B-Complex Vitamins, *Molecules*, 2020, **25**(18), 4041.
95 S. M. Choi and E. J. Shin, The Nanofication and Functionalization of Bacterial Cellulose and Its Applications, *Nanomaterials*, 2020, **10**(3), 406.
96 S. Jung, W. Kim and H. Y. Kim, Dynamics of directional soluble wicking, *J. Fluid Mech.*, 2021, **15**, A58.
97 H. Sang, H. Jin, P. Song, W. Xu and F. Wang, Gallic acid exerts antibiofilm activity by inhibiting methicillin-resistant Staphylococcus aureus adhesion, *Sci. Rep.*, 2024, **14**(1), 17220.
98 L. Hernandez-Pastor, J. Geurtsen, B. Baugh, A. C. El Khoury, N. Kalu, M. Gauthier-Loiselle, *et al.*, Clinical burden of invasive Escherichia coli disease among older adult patients treated in hospitals in the United States, *BMC Infect. Dis.*, 2023, **23**(1), 550.
99 J. Biswas, K. P. Appasami, H. Gautam, S. Mohapatra, S. Sood, B. Dhawan, *et al.*, Tick-tock, beat the clock: comparative analysis of disc diffusion testing with 6-, 10-, and 24-h growth for accelerated antimicrobial susceptibility testing and antimicrobial stewardship, *Eur. J. Clin. Microbiol. Infect. Dis.*, 2023, **42**(8), 929–943.
100 A. Rogers, K. Bullard, A. Dod and Y. Wang, Bacterial Growth Curve Measurements with a Multimode Microplate Reader, *Bio-Protoc.*, 2022, **12**(9), e4410.
101 V. Righi, M. Starkey, G. Dai, L. Rahme and A. Tzika, Magnetization transfer contrast MRI in GFP-tagged live bacteria, *Mol. Med. Rep.*, 2018, **19**(1), 617–621.
102 M. Hinnu, M. Putrinš, K. Kogermann, N. Kaldalu and T. Tenson, Fluorescent reporters give new insights into antibiotics-induced nonsense and frameshift mistranslation, *Sci. Rep.*, 2024, **14**(1), 6883.
103 K. Rajamanickam, J. Yang and M. K. Sakharkar, Gallic Acid Potentiates the Antimicrobial Activity of Tulathromycin Against Two Key Bovine Respiratory Disease (BRD) Causing-Pathogens, *Front. Pharmacol.*, 2019, **9**, 1486.
104 K. Dechsri, C. Suwanchawalit, P. Patrojanasophon, P. Opanasopit, S. Pengnam, T. Charoenying, *et al.*, Photodynamic Antibacterial Therapy of Gallic Acid-Derived Carbon-Based Nanoparticles (GACNPs): Synthesis, Characterization, and Hydrogel Formulation, *Pharmaceutics*, 2024, **16**(2), 254.
105 F. R. Ulhuq and G. Mariano, Bacterial pore-forming toxins, *Microbiology*, 2022, **168**(3), 1154.
106 A. Basnet, B. Tamang, M. R. Shrestha, L. B. Shrestha, J. R. Rai, R. Maharjan, *et al.* Assessment of four in vitro phenotypic biofilm detection methods in relation to antimicrobial resistance in aerobic clinical bacterial isolates. Jomehzadeh N, editor, *PLoS One*, 2023, **18**(11), e0294646.
107 C. L. Romanò, D. Romanò, I. Morelli and L. Drago, in *A Modern Approach to Biofilm-Related Orthopaedic Implant Infections: Advances in Microbiology, Infectious Diseases and Public Health*, Springer International Publishing, Cham, 1st edn, 2017, vol. 5, ch. 1, pp. 1–14.
108 F. Oustadi, E. D. Stephens and M. Badv, One-Pot Fabrication of Highly Flexible Fluorine-Free Lubricant-Infused Poly(vinyl alcohol) Films with Superior Antifouling Properties, *ACS Appl. Mater. Interfaces*, 2024, **16**(49), 67385–67398.
109 Y. Zhang, X. Wang, B. Lu, Y. Gao, Y. Zhang, Y. Li, *et al.*, Functional and binding studies of gallic acid showing platelet aggregation inhibitory effect as a thrombin inhibitor, *Chin. Herb. Med.*, 2022, **14**(2), 303–309.
110 O. M. Al-Amer, The role of thrombin in haemostasis, *Blood Coagulation Fibrinolysis*, 2022, **33**(3), 145–148.
111 S. Park and J. K. Park, Back to basics: the coagulation pathway, *Blood Res.*, 2024, **59**(1), 35.
112 S. S. Chang, V. S. Y. Lee, Y. L. Tseng, K. C. Chang, K. B. Chen, Y. L. Chen, *et al.*, Gallic Acid Attenuates Platelet Activation and Platelet-Leukocyte Aggregation: Involving Pathways of Akt and GSK3 β, *Evidence-Based Complementary Altern. Med.*, 2012, **2012**, 1–8.
113 J. L. Brash, T. A. Horbett, R. A. Latour and P. Tengvall, The blood compatibility challenge. Part 2: Protein adsorption phenomena governing blood reactivity, *Acta Biomater.*, 2019, **94**, 11–24.
114 L. Deng, Y. Qi, Z. Liu, Y. Xi and W. Xue, Effect of tannic acid on blood components and functions, *Colloids Surf., B*, 2019, **184**, 110505.
115 A. Kanpiengjai, C. Khanongnuch, S. Lumyong, D. Haltrich, T. H. Nguyen and S. Kittibunchakul, Co-production of gallic acid and a novel cell-associated tannase by a pigment-producing yeast, Sporidiobolus ruineniae A45.2, *Microb. Cell Fact.*, 2020, **19**(1), 95.
116 V. Vagenende, M. G. S. Yap and B. L. Trout, Mechanisms of Protein Stabilization and Prevention of Protein Aggregation by Glycerol, *Biochemistry*, 2009, **48**(46), 11084–11096.